Electronic Supplementary Material (ESI) for Sustainable Energy & Fuels.

Supplementary information

Film defect formation

After the PLD LSC8020 film deposition the high vacuum chamber was filled with oxygen (600 Torr) and the sample was cooled down at a cooling rate of ~~5~~ 10 ^{o}C/min to minimize any thermally induced defect formation. The silicon substrate and LSC material have two very different thermal expansion coefficients: 2.7 x 10^{-6} $^{o}K^{-1}$ [1] and 19.1 x 10^{-6} $^{o}K^{-1}$ [2] respectively. During cooling, due to the large difference in thermal expansion, the LSC film contracts faster than the silicon substrate, Fig.1S.

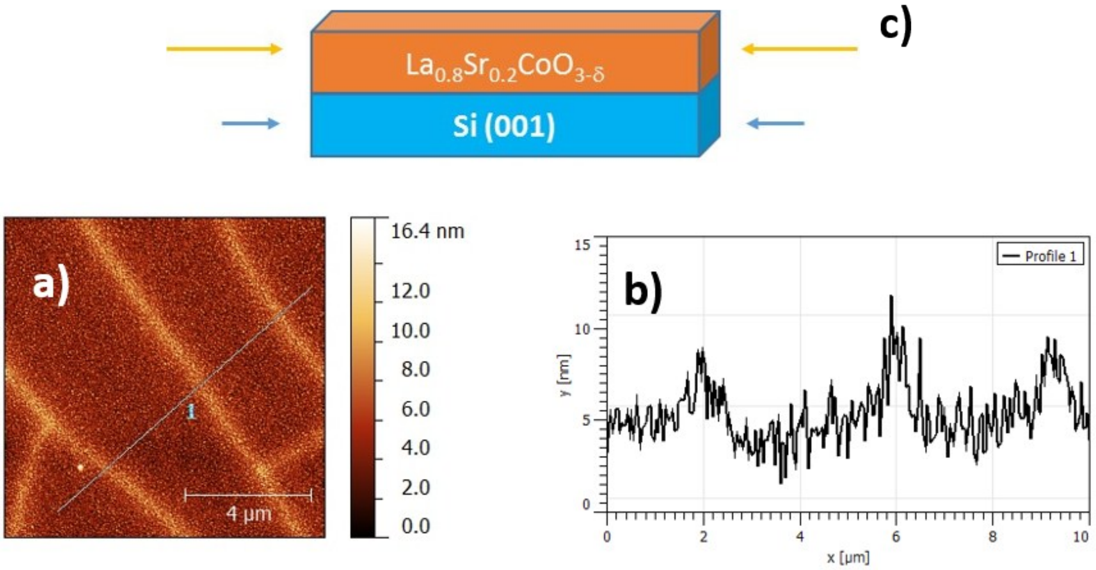

Fig.1S (a) AFM surface profile of a LSC/Si sample. AFM surface analysis of a LSC/Si sample grown at 600 ^{o}C. The line marked one corresponds to a line profile. The bright lines on the surface are corrugation of the film surface of around 3 nm high as can be observed by the profile in (b). During the sample cooling step to RT, the LSC film material is shrinking quicker than the silicon substrate producing compressive forces in the film as represented in the schematic (c).

Because of these forces local deformations appear all over the film surface. The density of these defects is inversely proportional to the PLD deposition temperature as shown in Fig.2 (main text). From the AFM analysis profiling Fig.1S (a,b) it is clear that the defects are deformed material (surface corrugations) and not open surface-cracks. In some cases when the cooling rate is too fast the surface corrugations can break to form cracks as shown in Fig.2S (LSC8020/SiO_{2sub} sample). All the samples employed on the IEDP experiments have been first screened by AFM to exclude the presence of open-cracks that could strongly affect the isotopic exchange results. When possible, for the sample synthesized at lower temperature, the FIB-SIMS analysis after the isotopic exchange step was performed inside an area free of defects; see for example the LSC/SiO_2 sample shown in Fig.2S. For the film with a higher defect density such as the one prepared at 750 ^{o}C, it was impossible to avoid the corrugated area since the SIMS analysis area was always maintained 15 x 15 μm^2.

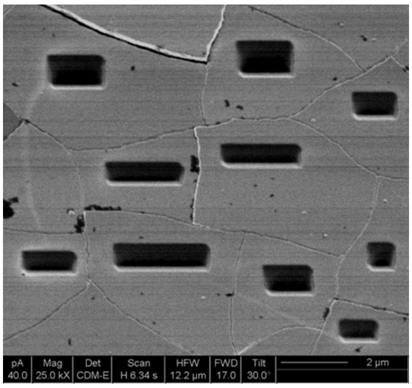

Fig.2S SE image of LSC/SiO_2 sample surface after FIB-SIMS analysis. SEM image obtained from a cracked LSC film after the depth profile analysis by FIB-SIMS. The analysis has been performed in crack-free areas.

X-ray-reflectivity (XRR) measurement

Two samples, one amorphous grown at 400 ^{0}C and one crystalline grown at 550 ^{0}C, have been analysed by the XRR technique. The PANalytical software package (X' Pert Reflectivity) has been employed to calculate the densities of the films of 300 nm thickness. In Fig.3S the two analyses are presented.

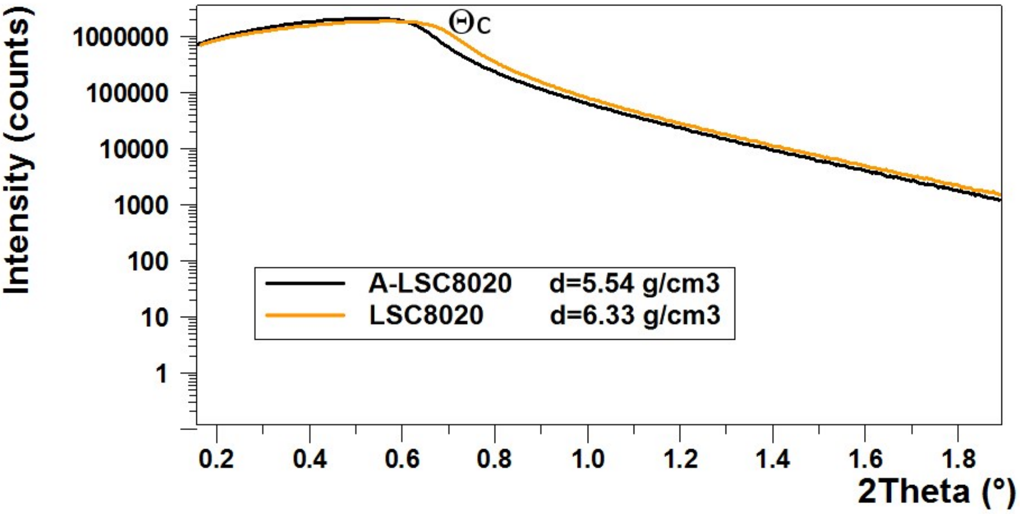

Fig.3S XRD analysis of 300nm thick LSC crystalline and amorphous films. The crystalline sample is represented in orange and the amorphous sample is shown in black. The critical angle value (Θ_C) is higher for the crystalline sample indicating a higher density.

The critical angle Θ_c can be defined as the angle beyond which the condition for the total reflection is no longer valid.

Low Energy Ion Scattering (LEIS)

The LEIS high vacuum chamber has an operating pressure of 10^{-8} mbar produced by the noble gas flux during LEIS experiments. Three noble gas sources were available: helium, argon and neon. The choice of the primary ion is conditioned by the mass of the chemical species to be analysed. Helium for example is used when the presence of light mass contaminants on the sample surface, like carbon or sodium, are also important for the investigation. The selected noble gas is ionized, mass selected, focused and rastered on the sample surface. Primary ions are at normal incidence to the target surface. Only the primary ions scattered by the sample surface through 145° are accepted by the Qtac100 analyser (a double toroidal electrostatic analyser-DTA). The very large acceptance solid angle together with parallel energy detection offers 3000 times higher sensitivity than conventional ion scattering spectrometers. In the case of insulating samples, to prevent any charging effects, low-energy electrons (10 eV) are flooded over the sample during the measurement. The secondary argon ion sputtering gun (energy 500 eV) is oriented at 59° with respect to the analysed surface. It is generally used alternating with the analysis beam to obtain a complete 3D-depth-profiling chemical map of the sample. The sputtered area was double the size of the analysed area. For this study the ^{4}He primary ion source with energy of 3 keV has been employed, the analyser pass energy was maintained at 3000 eV in all the experiments. In a typical LEIS spectrum each peak is produced by the binary collision between the primary ions and the atomic species at the sample surface. The energy peak position can be calculated according to the laws of conservation of energy and momentum knowing the solid angle of the analyser and the incident primary ion energy.[3] The element signal intensity is directly related to the amount of that particular atomic species on the analysed sample surface. Generally, the LEIS technique does not suffer from matrix effects nevertheless the ion yield corresponding to the interaction of the primary ion with the different chemical species could be different for each pair and a direct compositional quantification is not possible. To fit the LEIS surface scattering gaussian peaks a complex function that takes into account the very particular LEIS spectral background is employed. In Fig. 4S the cobalt, strontium and lanthanum normalized intensities for four LSC samples prepared at 400, 500, 600 and 750 °C by PLD are presented.

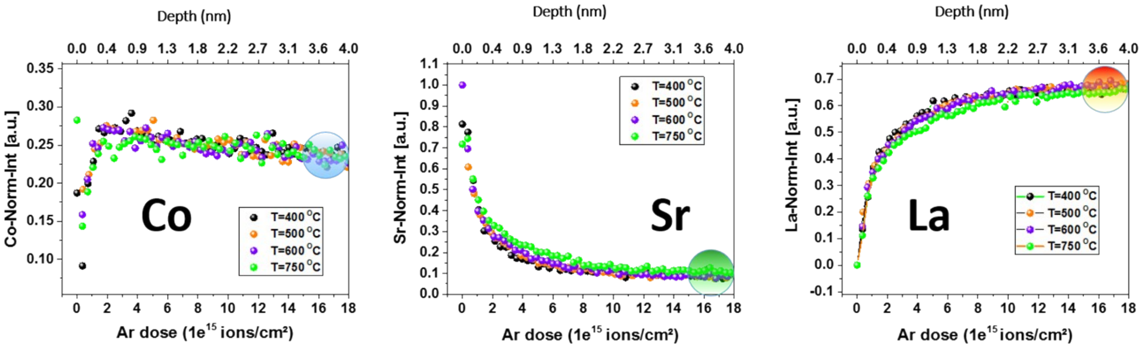

Figure 4S LEIS analysis of the 300 nm LSC films. Each of the different cation species intensity, cobalt, strontium and lanthanum from left to right, are represented for LSC films deposited at different temperatures. Each intensity has been normalized by the sum of all cations.

For each species, the element concentration has been calculated assuming that the normalized intensity at the plateau (marked with a circle) has the stoichiometric material composition. The second important assumption we have made is the absence of preferential sputtering of the sample by the argon ions.

DC-resistivity measurement

Fig. 5S shows the conductivity measurements obtained in a Van der Pauw configuration for five different LSC-8020 samples deposited on silicon substrates. Each film has a thickness of 300 nm and was grown by PLD in the temperature range of 200 ^{0}C-750 ^{0}C.

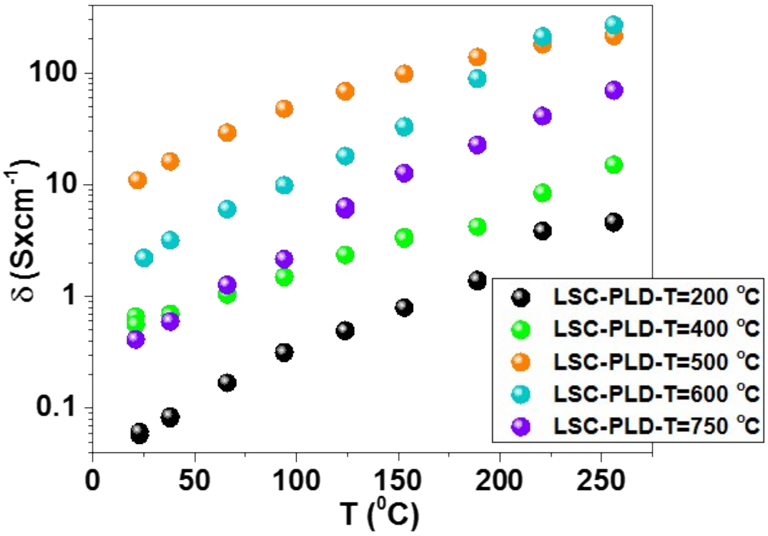

Figure 5S DC conductivity of different LSC films prepared at different deposition temperature. The amorphous LSC films (400 ^{o}C and 200 ^{o}C) present a sharp reduction of the electronic conductivity compared with the crystalline ones.

A Linkam chamber with four probes has been used for the analysis. The chamber has a little round furnace and the sample is placed on top of it. The temperature presented in the DC conductivity plot has been measured after the analysis on the sample surface by a thermocouple. Due to the large difference between the nominal chamber temperature and real one the maximum analysis temperature was around 260 ^{o}C. Whereas the Van der Pauw configuration is very sensitive to material defects, the values presented here will be used only for qualitative reasoning. The amorphous films (400 ^{o}C and 200 ^{o}C) clearly show a major decrease of the LSC8020 material conductivity with respect to the crystalline ones. It is worth pointing out how the film with higher defect density (750 ^{o}C) presents an intermediate conductivity value related to the presence of the defects themselves.

Isotope exchange of Amorphous-cathodes thin films

Once the samples have been isotopically exchanged, depth profile analysis was performed in a dynamic FIB-SIMS. The calculated oxygen-18 isotopic fraction has been fitted with the sheet solution to Fick's diffusion equation to calculate the values of D* and k*. For each sample the analysis has been repeated between 6 and 8 times. To analyse this large amount of data we employed TraceX, a software package developed to run in the Matlab environment.

An example of the fit for ALSC8020, ALSC6040, ALSC214 and ALSMC are presented in Fig. 6S.

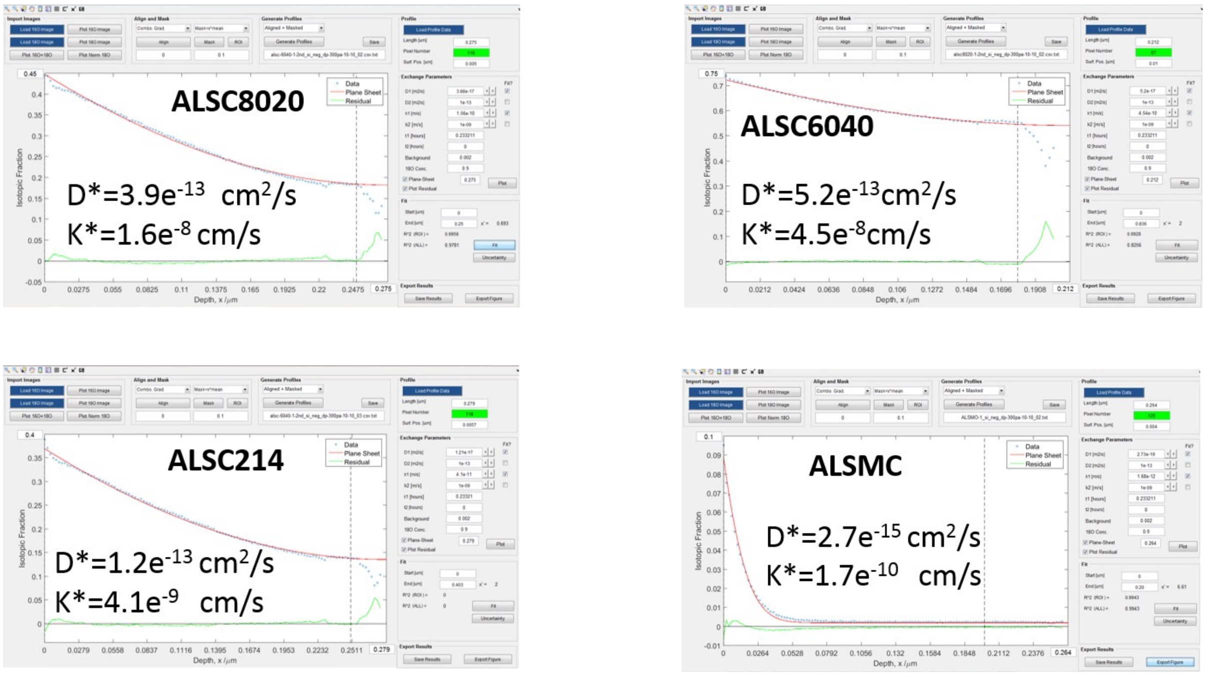

Figure 6S Oxygen-18 isotopic fraction diffusion profiles analysed by TraceX. One single analysis for each of the different cathode samples have been here presented. The film surface is on the left side and the interface between the cathode film and the Si crystal is on the right where the oxygen fraction (blue dots) drops.

Blue dots are the original data, in red is represented the sheet solution fitting and in green the residual. The standard error for D* and k* calculated from the different measurements on a single sample vary from 1-3% for the D* and 4-9% for the k*. Due to the large dot size employed in the main text figure the errors have not been included. We also identified an extra experimental error source affecting the oxygen self-diffusion constants calculation in the residual gas of the SIMS chamber that could be different from session to session. This error could cause an underestimation of the real constant values and it has been estimated at a maximum of 10%.

Symmetric Amorphous-LSC cell characterization

PLD-LSC8020 300 nm films have been deposited at room temperature on both sides of an YSZ commercial substrate (230 µm).The voltage applied during the AC-impedance analysis has been maintained at 10 mV. To avoid any positive catalytic contribution from the current collector material, a gold mesh has been employed. In all spectra collected in the range of 338 ^{o}C-415 ^{o}C, four different arcs are recognizable Fig. 7S. Each semi-circle is depressed and differs from the expected perfect semi-circle shape. This could be related to the reduced electronic conductivity of the LSC8020 amorphous films combined with the use of a gold mesh current collector (mesh size 1 mm^{2}). The increase of sheet resistance can provoke an inhomogeneous electrical field over the sample during the AC measurements. The impedance complex plane Nyquist plot is described by four different features: a high frequency arc attributed to the YSZ electrolyte grain resistance, a middle-high frequency arc attributed to the YSZ grain boundary resistance, a middle-low frequency arc corresponding to YSZ/LSC interface resistance (R_i) and the low frequency arc related to the cathodic resistance (R_p). The capacitors associated with each resistance have been replaced by the more general constant phase elements CPE.

$$Z_{CPE} = \frac{1}{Q \cdot (i \cdot \omega)^n}$$

For fitting the experimental impedance data, the model described by Baumann *et al.*[4] for a dense perovskite mixed conducting film on an YSZ electrolyte has been chosen. The relative permittivity, ε', of YSZ has been estimated to be 30 as reported in [5]. Using this value it is possible to calculate the expected area specific bulk capacitance for the 230 μm thick YSZ electrolyte according to Eq.1

$$\mathrm{C} = \frac{\varepsilon' \cdot \varepsilon_0}{l}$$

where ε_0 is the permittivity of free space, $8.854 \cdot 10^{-14}$ F/cm, and l is the thickness of the YSZ substrate. The calculated capacitance is in the order of 1.15×10^{-10} F/cm^2 consistent with the experimental value of the first arc reported in Table 1S (2×10^{-10} F/cm^2). The experimental grain boundary capacitance of 5.8×10^{-7} F/cm^2 is also consistent with values reported in the literature.[6] The interface resistance R_i, corresponds to the phenomena of O^{2-} transfer across the LSC-electrode/YSZ interface. The related capacitance CPE_i, is generally described as a double layer capacitance produced by the block of electronic charges at the interface with the electrolyte. The experimental interface capacitance, Table 1S, is around 40 μF/cm^2 measured at 365 °C of the same order of magnitude as the capacitance reported by Baumann for a LSCF film at 500 °C.

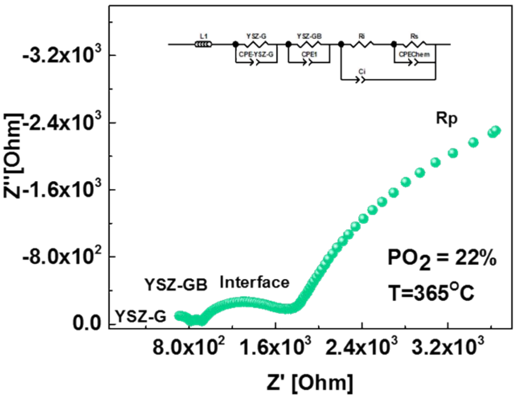

Figure 7S EIS analysis of a symmetric cell ALSC/YSZ/ALSC sample. The sample has been measured under 10mV at 365 °C and 22% of $p(O_2)$.

As concluded by Baumman *et al.* this value is too high to be related only to an electrostatic double layer capacitance and a chemical change at the interface should be responsible for it. Finally, the dominant resistive process R_p observed at low frequency is associated with the oxygen exchanged at the surface of the electrode. The large capacitance referred to as a chemical capacitance (CPE_{chem}) is associated with the oxygen stoichiometry changes in the bulk of the electrode.[7]

The CPE values in Table 1S have been converted to pure capacitances using the following equation:

$$C = (R^{1-n} \cdot Q)^{1/n}$$

Where R is the resistance, Q is the constant phase element (CPE) and n is the parameter that determines how close the constant phase is to a pure capacitance (n=1).

Table 1S Capacitances measured by EIS analysis performed at 365 °C and pO_2 22%

Conditions	YSZ-Grain Interior	YSZ-Grain Boundaries	LSC-YSZ Interface	R_p
T=365°C	Arc I (C F/cm^2)	Arc II(C F/cm^2)	Arc III (C F/cm^2)	Arc IV (C F/cm^2)
PO_2=22%	2.00×10^{-10}	5.81×10^{-7}	4×10^{-5}	0.022

The critical length value L_c defined as D^*/k^* will determine if the cathodic resistance is mainly dominated by the cathode surface (when $L_c <<$ cathode thickness) and any oxygen bulk diffusion limitations can be ignored. Employing the D^* and k^* experimental values (Table 1 main text) the critical length in the exchange conditions used is L_c=243 nm. The film thickness is around 300 nm so very close to the L_c; bulk diffusion limitation cannot be dismissed *a priori*. In Fig. 8S the activation energies calculated for the four different resistive processes measured by AC impedance in pO_2 22% have been presented.

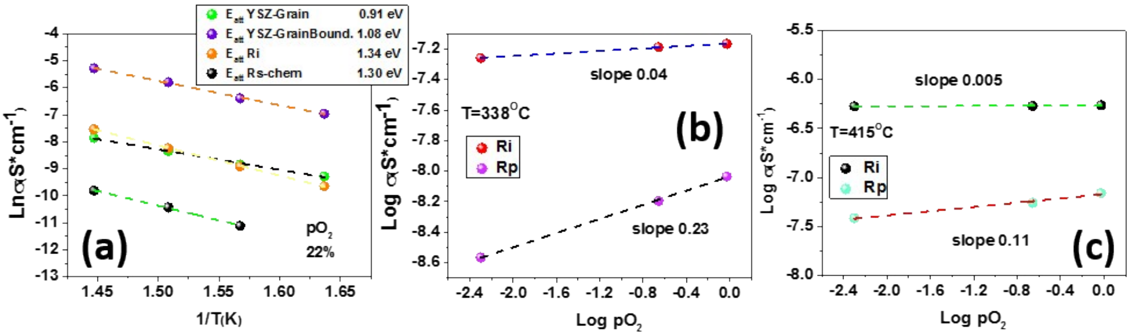

Figure 8S EIS activation energy and pO_2 dependence studies. a) The activation energies for the YSZ-bulk YSZ-grain boundaries, R_i and R_p have been calculated. (b,c) The pO_2 dependence (m) have been obtained for Ri and Rp at 338 °C and 415 °C. A decrease of m with the increasing measure temperature has been observed.

The activation energy for the bulk and YSZ grain boundaries are in agreement with the values reported in the literature. The cathodic resistance Rp displays an activation energy of 1.3 eV similar to the one calculated for Co-rich MIECs materials (≈1.3 eV) [4]. The conductivity dependence of the interface resistance Ri with the pO_2, Fig.8S (b), is very low (0.03) as expected. The dependence of the R_p with the pO_2 instead is changing with the temperature going from m=0.23 (~1/4) at 338 $^{\circ}$C to m=1.11 at 415 $^{\circ}$C (~1/8).

Gold grid deposited on the ALSC cathode

For the fuel cell test of Ni-YSZ/YSZ/ALSC a Pt current collector was used on the thick porous anode while a gold grid was sputtered on the side of the dense 300 nm thick amorphous cathode. Gold, when in bulk, is not active for oxygen reduction. The optical image after the analysis, Fig. 9S, has been used to calculate the free ALSC cathode surface.

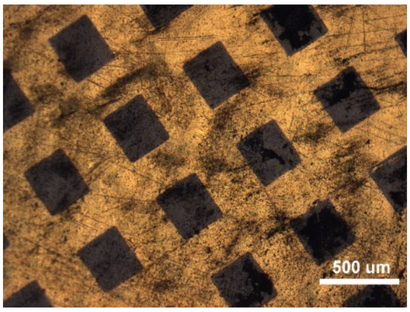

Figure 9S Optical microscope image of the gold grid on ALSC cathode. The cathode free surface represents roughly 25% of the total cathode surface.

References

[1] Y. Okada, Y. Tokumaru. Precise determination of lattice parameter and thermal expansion coefficient of silicon between 300 and 1500 K. *Journal of Applied Physics* 56, 314 (1984).

[2] F. Tietz, I. Arul Raj, M. Zahid, D. Sto ̈ver. Electrical conductivity and thermal expansion of $La_{0.8}Sr_{0.2}(Mn,Fe,Co)O_{3-y}$ Perovskites. *Solid State Ionics* 177, 1753 – 1756 (2006).

[3] H. Niehus, W. Heiland, E. Taglauer. Low-energy Ion Scattering at Surfaces. *Surf. Sci. Rep.* 17, 213–303 (1993).

[4] F.S. Baumann, J. Maier, J. Fleig. The polarization resistance of mixed conducting SOFC cathodes: A comparative study using thin film model electrodes. *Solid State Ionics* 179, 1198–1204 (2008).

[5] F.E.G. Henn, R.M. Buchanan, N. Jiang, D.A. Stevenson. Permittivity and AC conductivity in yttria-stabilized zirconia. *Appl. Phys. A* 60, 515 (1995).

[6] J. Nielsen, J. Hjelm. Impedance of SOFC electrodes: A review and a comprehensive case study on the impedance of LSM: YSZ cathodes. *Electrochimica Acta* 115, 31– 45 (2014).

[7] F.S. Baumann, J. Fleig, H.U. Habermeier, J. Maier. Impedance spectroscopic study on well-defined $(La,Sr)(Co,Fe)O_{3-\delta}$ model electrodes. *Solid State Ionics* 177, 1071–1081 (2006).